

Hydrodynamic parameter optimization for miniature underwater glider wings

Moustafa Elkolali

Department of Mechanical,
Electronic and Chemical
Engineering
Oslo Metropolitan University
Oslo, Norway
elkolali@oslomet.no

Wilfried Arnaud Splawski

Department of Material
Engineering
ENIT ecole national d'ingenieur
de Tarbes
Tarbes, France
wsplawsk@enit.fr

Alfredo Carella

Department of Mechanical,
Electronic and Chemical
Engineering
Oslo Metropolitan University
Oslo, Norway
alfcar@oslomet.no

Alex Alcocer

Department of Mechanical,
Electronic and Chemical
Engineering
Oslo Metropolitan University
Oslo, Norway
alepen@oslomet.no

Abstract— This paper describes the design and optimization of the shape of the wings of “OASYS” research project underwater glider, by maximizing the lift to drag ratio through using computational fluid dynamics. Different wing layouts were examined based on the resulting lift and drag forces. The best NACA profile for this application was selected based on the lift and drag coefficients, the stall angle and the angle of attack that generates the highest lift to drag ratio. The shape of the wing was then determined by examining the effect of the sweep angle, front and back tapering angles, and the combination of the two on total lift and drag forces. Two dimensional and three-dimensional simulations were performed in “XFOIL” and “ANSYS Fluent” software, the type of simulation depending on the property examined. This resulted in 91 simulations. The results of each wing layout were assessed based on lift forces, drag forces, and the ratio between the two.

Keywords—micro underwater glider, hydrodynamic characteristics, wing geometry, computational fluid dynamics.

I. INTRODUCTION

The high cost of ocean observation systems remains one of the obstacles to a better understanding and sustainable development of maritime scientific activities. “OASYS”, which stands for Ocean-Air synoptic operations using coordinated autonomous robotic SYStems and micro underwater gliders, is a project that is aimed at designing and developing a fully automated robotic system, which can significantly reduce ocean observation and monitoring costs. The project proposes a system that consists of a swarm of Micro Underwater Gliders (MUGs), which can operate autonomously with the aid of Unmanned Aerial Vehicles (UAVs) and an Unmanned Surface Vessel (USV). The two supporting systems will minimize human intervention, by making deployment, recovery, charging, communication and data collection fully automated. The proposed “OASYS” system is shown in Fig. 1.

Underwater gliders are autonomous vehicles which change their buoyancy to perform vertical cycles, and utilize wings to develop forward motion from this vertical motion. The wings provide a lift force, which acts perpendicular to the movement path. The resultant of the vertical buoyancy force and the wing generated lift is a saw tooth movement.

Underwater gliders can have deployment durations of months and deployment ranges of thousands of kilometers. Traditional Autonomous Underwater Vehicles (AUVs) have durations of days [1]. “OASYS” project aims to use a MUG that

has a maximum weight of 3 kg, so that it can be deployed and recovered autonomously using a multirotor UAV. This will reduce the cost and effort of traditional deployment and recovery. The main tasks of the glider include measuring ambient water properties such as temperature, salinity, and CDOM (Colored Dissolved Organic Matter). The gliders used in “OASYS” should have as wide a horizontal range as possible. The efficiency of the glider is therefore the horizontal distance traveled divided by energy consumed on the trip.

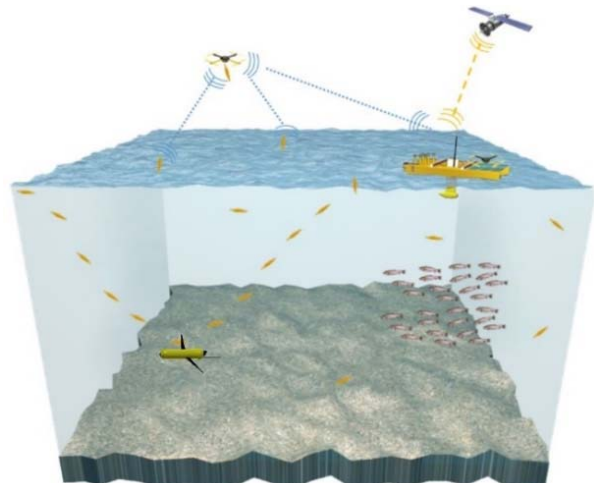


Fig. 1. Concept of “OASYS” project

The efficiency of the glider depends on its working depth and speed. Working in a shallow environment is less efficient, as the glider has to alter its buoyancy more often by activating the buoyancy engine, which consumes battery power. The glider therefore has to perform more cycles to travel a horizontal distance than it would for a deeper cycle, as shown in Fig. 2.

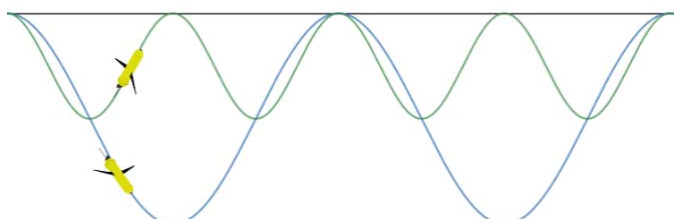


Fig. 2. Deeper glider cycles vs. shallower cycles

Glider efficiency also depends on speed, slow speeds being efficient. Slow movement requires only a small buoyancy force. The buoyancy engine therefore works for shorter periods of time and so consumes less energy. Higher glide speeds also mean higher drag forces on the hull, which will be further explained in the paper. Efficiency assumes that gliders have enough speed to overcome sea currents.

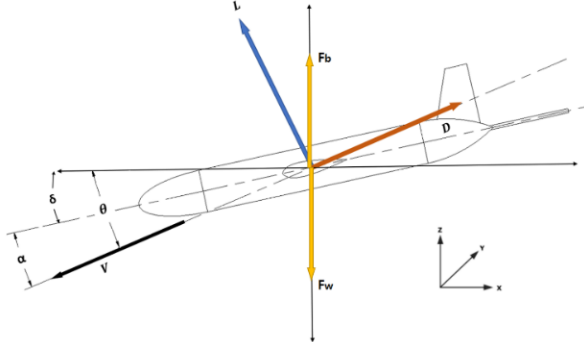


Fig. 3. Forces acting on an underwater glider

Fig. 3 shows the forces that act on an underwater glider during dives, and their directions. L marked by the blue arrow is the lift force, D marked by the red arrow is the drag force, F_b is the buoyancy force and F_w is the weight force, both marked by yellow arrows, and V is the direction of the velocity of the glider, its direction marked by the black arrow. θ is the gliding angle, and α is the angle of attack, the difference between them being the pitch angle, denoted by δ .

The wings of the glider are the main provider of lift force. The geometry therefore has to be optimized to provide the best L/D ratio, and hence higher efficiency. This efficiency is translated into a higher range and duration of a glider with fixed battery life.

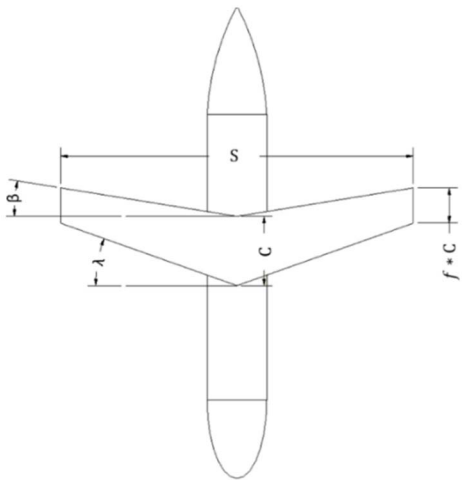


Fig. 4. Geometrical parameters of the glider's wings

Fig. 4 shows the geometrical parameters of the wing. C is the chord, S is the total span of the wing, λ is the sweep angle, f is the taper factor, and β is the back taper angle. The parameter β is based on λ and f .

The profile used in this work is the symmetrical National Advisory Committee for Aeronautics (NACA) profile. Wing

profiles that are not symmetrical or profiles that are not aligned with the longitudinal axis of the glider, will generate an additional component of lift in one direction of the cycle. The dive of the glider will therefore not be symmetrical, unless it is able to roll 180°, this roll being performed twice every cycle. This will be further examined in section II.

Different symmetrical NACA profiles (NACA-0015, NACA-0025, and NACA-0035) were studied by [2], the focus of the study being on the stall angle of each profile. It was noted that stall angle increases, and coefficient of lift decreases with thickness, an increment in the separation point oscillation amplitudes occurring. Reference [3], however, examined the best wing geometry for the SLOCUM commercial glider at different angles of attack, and concluded that the NACA profile wing could improve the hydrodynamic characteristics of the SLOCUM glider. Reference [4] was aimed at using the glider as an underwater payload delivery system and optimized the wing geometry for this use. The effect of using a rectangular and a tapered wing on lift, drag, and the stability of the glider was studied. However, they used the same span in their simulations and the areas of the rectangular and tapered forms are therefore not the same. The rectangular form showed higher lift generation as it has a larger area, the tapered form showing better stability on the glider.

The effect on glider performance of adding a winglet to the tip of the wing was studied and simulated by [5]. Their study has shown that winglets give an increase of 6.3% in gliding speed and 2.2% in gliding ratio.

II. TWO-DIMENSIONAL ANALYSIS

A. Type of profile

The first step in designing the glider wings was defining the wing cross-section. Some commercial gliders, such as the Slocum, use flat plates of small thickness, manufactured from carbon fiber to increase their strength, Fig. 5. Others use more efficient cross-sections, manufactured from either composites or lightweight polymers, such as the Seaglider, Fig. 6.

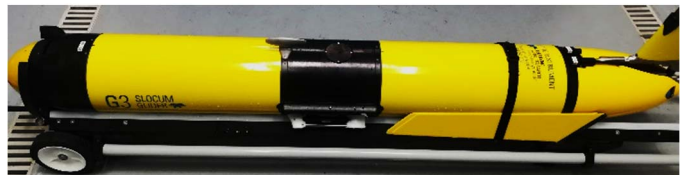


Fig. 5. Slocum G3 glider with detachable wings before deployment (image by the author)



Fig. 6. Seaglider wings cross-sections (image by the author)

SEAEDEXPLORER implemented the use of the “Wingless” design. The stern of the glider has four small wings in the shape of an “X” instead of a traditional wing, as shown in Fig. 7. This design eliminates the need for a fixed rudder, because the wings produce sway stability, which is the stability of linear movement on the Y-axis of the glider. The three principal axes are shown in Fig. 3. A further advantage of this design is a smaller wingspan, which helps avoid the glider wings being entangled or broken during launch, recovery, and operation. [6]



Fig. 7. SEAEDEXPLORER wingless design (image by the author)

NACA developed different types of aerofoil shapes for aircraft wings. These profiles have been adapted and used on many underwater vehicles [7]. This section aims to determine the most hydrodynamic efficient profile - the profile with the highest L/D ratio for the glider. There are, however, considerations other than hydrodynamic efficiency that should be taken into account. Weight is the strictest constraint in the design process, not just in wing design, but also for the entire glider. Not every cross-section is therefore suitable for such a concept. The second factor is the flow of water over the glider. The flow must be laminar across most of the areas of the glider, to reduce drag force while in motion. A speed of 0.2 m/sec ($\approx 0.4\text{kn}$) of the glider along its path, with a Reynolds number of 0.5×10^5 was chosen for all simulations, this speed being the speed that the glider is designed to operate at. This is slow compared with traditionally propelled AUVs, which can reach 1.5m/sec. Gliders have, however and as explained earlier, superior ranges and durations [8]. According to [9], the nominal speed of SLOCUM and Seaglider is 0.25 m/sec.

The NACA symmetrical cross-section was chosen as it provides the same characteristics while heading vertically up or down. The number of the profile has 4 digits, the first two defining the camber of the profile which in this case is two zeros, the second two digits describing the relative thickness of the profile. For example, a NACA-0015 is a profile that is symmetrical with a thickness of 15% of the chord of the wing. Fig. 8 shows different NACA profiles with the same chord.

The first factor to consider when assessing a profile is the relative thickness of the profile. The hydrodynamic efficiency of the NACA profile is particularly susceptible to profile thickness [2]. According to [11], the drag coefficient and lift coefficient of a body are directly proportional to the drag force and the lift force on the body, and inversely proportional to the projected area of a plane normal to the flow, velocity of the flow and density of the fluid.

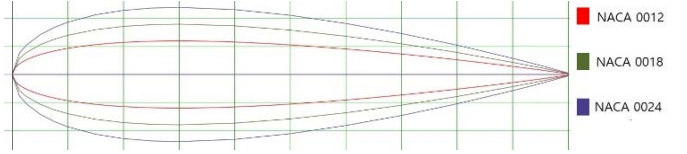


Fig. 8. Difference between cross-sections of NACA-0012, 0018, and 0024 according to [10]

Drag force is primarily divided into pressure drag force also called form drag, and skin drag force or simply friction drag. Pressure drag is to a great extent dependent on the shape of the body and can be reduced most effectively by geometric optimization. It is proportional to the frontal area and the pressure difference on the body in the direction of flow. Skin drag is proportional to the viscosity of the fluid, due to it being the result of shear stress on the wall of the body [11]. The majority of drag on a streamlined shape is from skin drag rather than pressure drag.

The angle of attack and the stall angle are two primary factors that also affect drag and lift coefficients. Stall angle is the angle at which the wing theoretically provides zero lift. This is not favorable, particularly if the wing has a wide range of stall angle. The stall angle of different profiles was found using XFOIL software and plotting values of CD, CL, and the ratio between them vs. the angle of attack α . The setup was tested before the software was used on the NACA profiles, by simulating the flow over a common geometry, so allowing it to be referenced and compared with textbook results. The geometry of a circular rod was simulated in XFOIL. The results are shown in table I and compared with results from [11].

TABLE I. COEFFICIENT OF DRAG RESULTS FROM XFOIL COMPARED WITH TEXTBOOK RESULTS FROM [11].

Geometry Simulated		<i>Circular Rod</i>	
<i>Type of flow</i>		Laminar ($R_e=2000$)	Turbulent ($R_e=1578532$)
<i>XFOIL</i>	<i>Friction drag</i>	$C_{df} = 0.49340$	$C_{df} = 0.00416$
	<i>Pressure drag</i>	$C_{dp} = 0.73027$	$C_{dp} = 0.29512$
	<i>Total coefficient of drag</i>	$C_D = 1.22367$	$C_D = 0.29928$
<i>Reference [11]</i>		$C_D = 1.2$	$C_D = 0.3$

Reference [12] compared experimental measurements with numerical simulations that used XFOIL and a low Reynolds number of around 2.0×10^5 . XFOIL showed promising results in the prediction of the coefficients of lift and drag, the authors recommending the use of the software for low speeds, due to its simplicity and ease of use. Reference [13] also showed the software to be useful and powerful in subcritical designs with low Reynolds number.

The validity of using XFOIL for low Reynolds numbers was determined by reviewing the literature stated earlier, and by validating the setup of the software. The five NACA profiles were then, after this, simulated. Fig. 9-12 shows the different hydrodynamic parameter values of the cross-sections, relative thickness ranging from 12 to 16%. The 5 profiles have dimensions that are compatible with the remainder of the design components. The profile is symmetrical. The hydrodynamic

parameters are therefore also symmetrical between the positive and the negative values of α shown in Fig. 9-12. Table II shows the maximum lift to drag ratio that can be obtained for each simulated profile and the corresponding angle of attack α .

TABLE II. MAXIMUM LIFT TO DRAG RATIO AND CORRESPONDING ATTACK ANGLE FOR DIFFERENT NACA PROFILES

NACA profile	0012	0013	0014	0015	0016
Max. L/D	24.40	24.92	25.30	25.42	25.87
α ($^{\circ}$)	5	5.5	6	6	6.5

NACA-0016 not only has the highest hydrodynamic efficiency, but also the highest stall angle. It was, for these reasons, chosen as the profile for the wing, despite NACA-0012 having the lowest weight, which can be considered to be a big advantage, as weight is as mentioned earlier crucial in the design process. This can, however, be mitigated by making the wings hollow. Material that is rigid enough will have sufficient hardness for a hollow design. Some polymers or composites also are low weight. Carbon fiber and glass fiber are examples of materials that can and have been used in the manufacture of these wings. Stereolithography, also known as SLA printing, can also be used in the manufacture of these wings, the resulting polymer having sufficient hardness, and relatively low density.

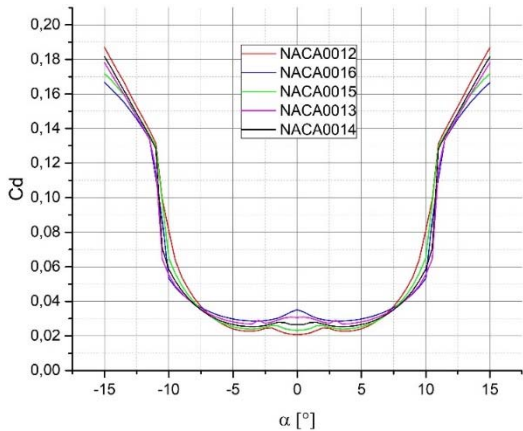


Fig. 9. Coeffecient of drag at different angles of attack

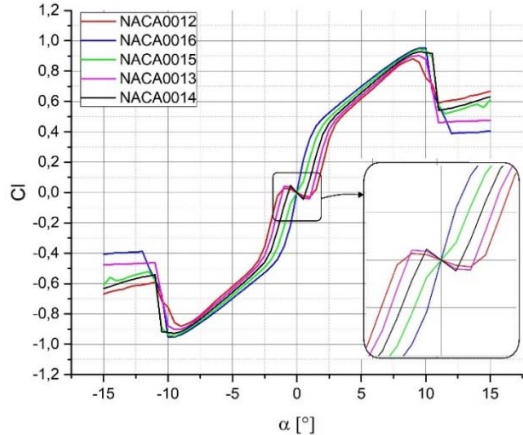


Fig. 10. Coeffecient of lift at different angles of attack

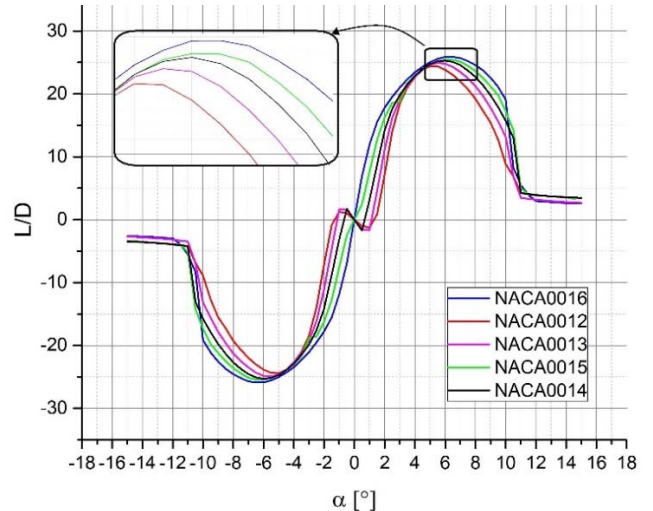


Fig. 11. Lift to drag ratio at different angles of attack

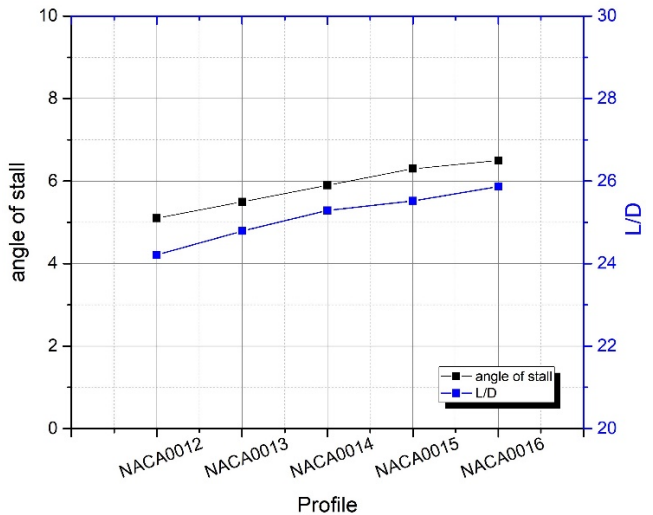


Fig. 12. Maximum lift to drag ratio and angle of stall for different symmetrical NACA profiles

B. Two-dimensional finite modelling

The next step after determining the most suitable profile, was to define the best chord for this profile. The ANSYS Fluent software was used in these simulations. Fig. 13 shows the geometry simulated in the software and the applied mesh.

There are three different regions with different mesh sizes. The first region is the region that contains the boundary layer around the body, and has the finest mesh. The second is the body of influence, which also covers the region behind the trailing edge, to capture all vortices and the separation point. The last region is where less change in parameters occurs, and therefore has the coarsest mesh to avoid wasting time and computational resources. The mesh domain has a height of 2 m and a maximum length of 3m. The maximum element edge size is 0.01 m in 2D simulations and 0.03 m in 3D simulations. The growth rate is set to 1.2.

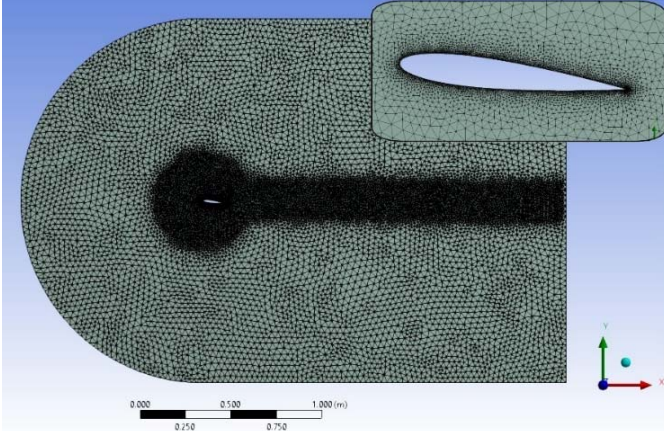


Fig. 13. Meshing setup of the 2D simulations

It is important in the 2D simulation to optimize the chord hydrodynamic parameters, irrespective of the area of the wing. This is because all setups have the same area. It should, however, be noted that 2D is not entirely accurate, as there are parameters that it does not take into consideration. These include induced drag, which is the drag resulting from a portion of the fluid moving from the higher-pressure region of the wing to the lower pressure region at the tip of the wing, depending on the direction of lift force. This results in a loss of lift force. Adding winglets to the tip of the wing can, however, reduce this effect significantly. The effect will be further examined in the following sections. Fig. 14-15 show the pressure contour and the velocity of the fluid around the wing cross-section in 2D simulation.

The chord range suitable for the design is from 80 mm to 120 mm. Every simulation was therefore performed 3 times, once on a chord length of 80 mm, then on one of 100 mm, and finally on a chord of 120 mm. Angle of attack is another parameter that was taken into account. Simulations were carried out for two angles, 6.5° and 0°, as the angle of attack that gives the highest efficiency for NACA-0016 is 6.5°. Simulating on 0° is important as well, because in some situations the glider may not be able to have an angle between the velocity vector and the pitch angle. It is therefore important that the controller system has lift and drag coefficients for 0°, to be able to adjust the behavior of the system and its response in this situation. Angle of attack is achieved by accurately moving the center of mass of the glider linearly in the longitudinal direction of the glider. This requires a sophisticated controller, and an accurate mechanical system. The slightest uncontrolled change internally from the system due to, for example, backlash or due to an external factor such as strong currents, will affect the pitch angle.

Another solution is that the wings are fixed at an angle of 6.5° to the axis of the glider. The wings will then have an angle of attack, while the glider has a 0° angle of attack. As mentioned earlier, the glider must be able to roll 180° each cycle to keep this angle constant while diving or surfacing.

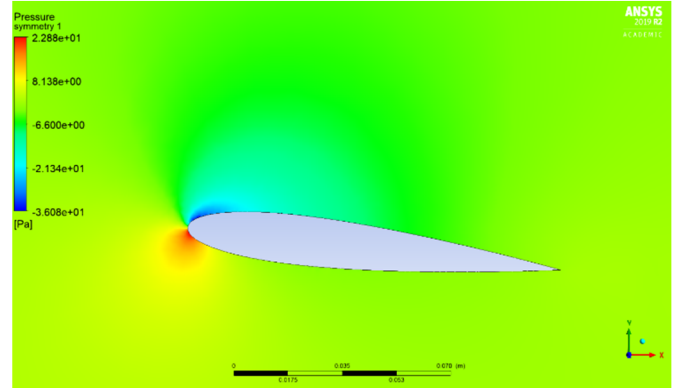


Fig. 14. Pressure contour for NACA-0016 with 100 mm chord at 6.5° angle of attack

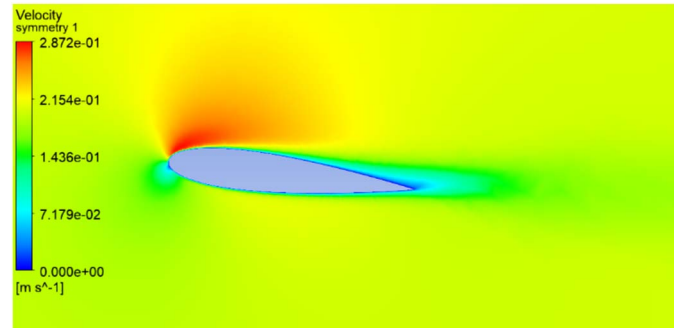


Fig. 15. Velocity contour for NACA-0016 with 100 mm chord at 6.5° angle of attack

Fig. 16 and 17 show the coefficient of drag, coefficient of lift, and lift to drag ratio for the setups described earlier. The chord with the least drag is 100 mm at $\alpha = 0^\circ$, while highest lift is for a chord of 120 mm at $\alpha = 6.5^\circ$.

One more important note from the 2D simulations is the considerable increase in lift force provided by the wing by increasing α to 6.5°. Drag also increases, but the overall L/D increases remarkably. The ratio increases for a 100 mm chord by a factor of approximately 180.

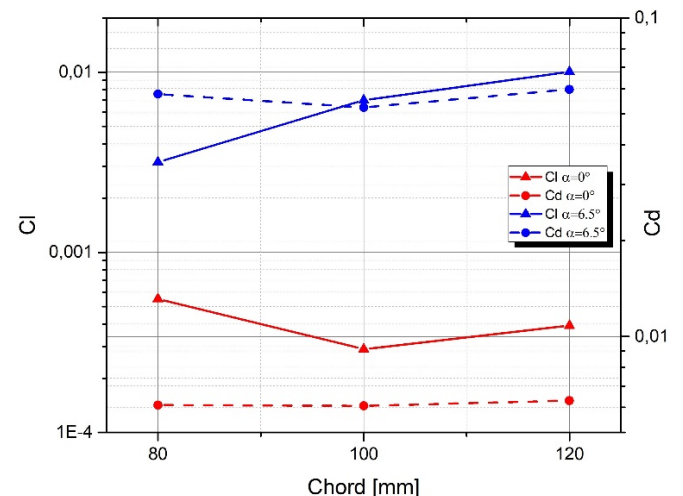


Fig. 16. C_l and C_d for the three chords simulated

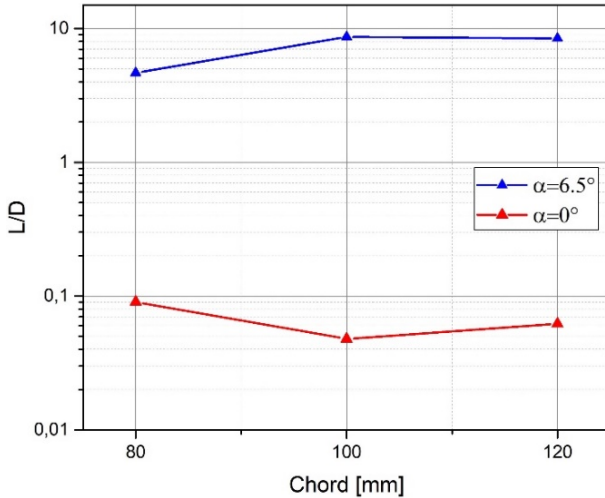


Fig. 17. L/D ratio for the three chords simulated, with logarithmic scale

III. THREE-DIMENSIONAL ANALYSIS

Three-dimensional analysis was used to simulate parameters that cannot be optimized in two-dimensional analysis. This includes the simple rectangular form, sweep angle, and both tapering angles, as explained before.

A. Rectangular Form

The rectangular form was first simulated as a basis for comparison with other 3D forms. It has a tapering factor $f = 1$, and a sweep angle, $\lambda = 0$. Fig. 18 shows the hydrodynamic parameters resulting from simulating the three different chord values determined earlier, at an angle of attack α of 0° and 6.5° .

The same span was used for all three chords. A 120 mm chord showed a higher L/D ratio, which differs from the results from 2D simulations. The same span was used in 3D simulations for all the chords. The bigger the chord, the bigger the area, and the higher the ratio. 3D analysis was not, as mentioned earlier, used to define the area. It was used to define the best geometry of the wing.

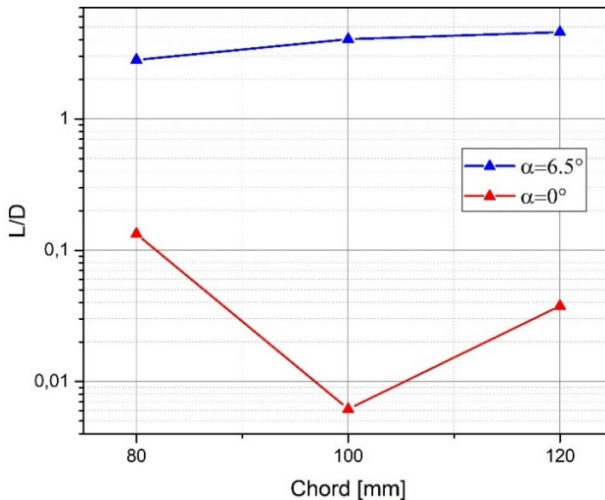


Fig. 18. L/D ratio of the rectangle form with logarithmic scale

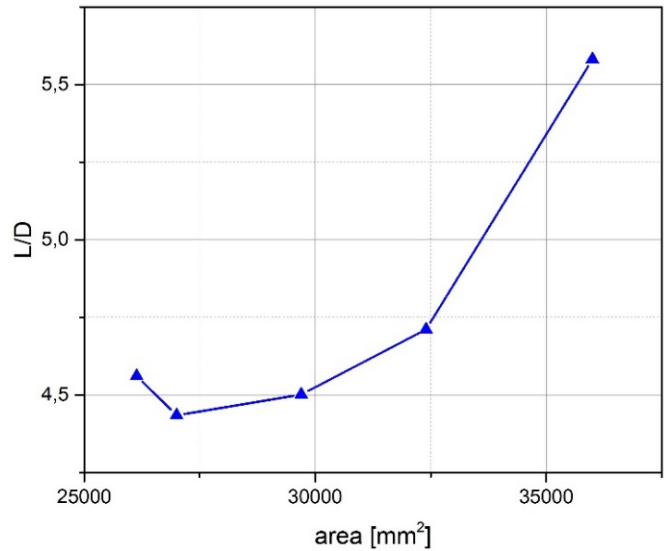


Fig. 19. Effect of increasing the area of the wing, by increasing the span on the L/D ratio

Fig. 19 shows the effect of increasing the area of the wing. The simulations showed that it is possible, at the beginning of the curve where area is less than 27000mm^2 , to obtain the same or even better parameters using a smaller area of the wing. However, in the second region, where the area is larger than 27000mm^2 the larger the area the higher the L/D ratio.

B. Sweeping

The second geometry simulated was the swept wing, see Fig. 4. Fig. 20 shows the three angles of λ simulated - 15° , 30° , and 45° . Only the effect of sweeping was studied. Angle β therefore equals λ . Simulations were also carried for the three chords, using an angle of attack α of 6.5° . Sweeping has a beneficial effect on drag, but a detrimental effect on wing lift. The resulting L/D ratio is, at some angles, also better. It should however be noted that lift generated by the wing was less than for 0° .

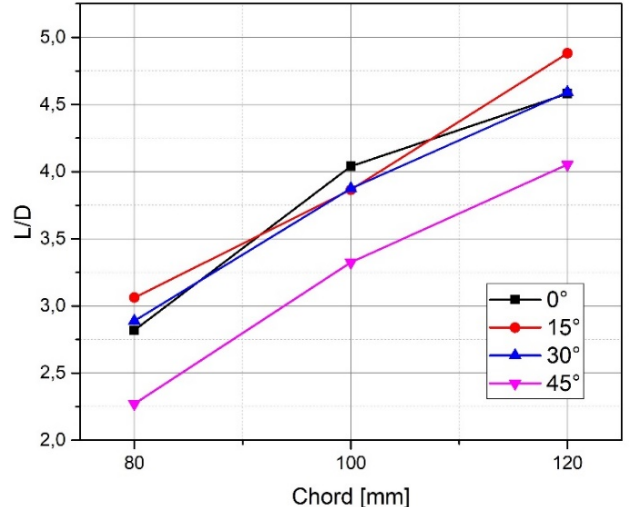


Fig. 20. Effect of sweeping the wing on the L/D ratio

C. Front Tapering

The tapering effect was simulated for values of f of 0.5, 0.65, and 0.8. The angle β was zero, as only front tapering was simulated, and all simulation geometries have the same area. It was noted that the lowest drag force is at $f = 0.5$, and the highest lift force was when the tapering factor equals 0.65. The highest L/D ratio was at $f = 0.65$. Fig. 21 shows a comparison of the parameters of the front tapering simulations from using the same area.

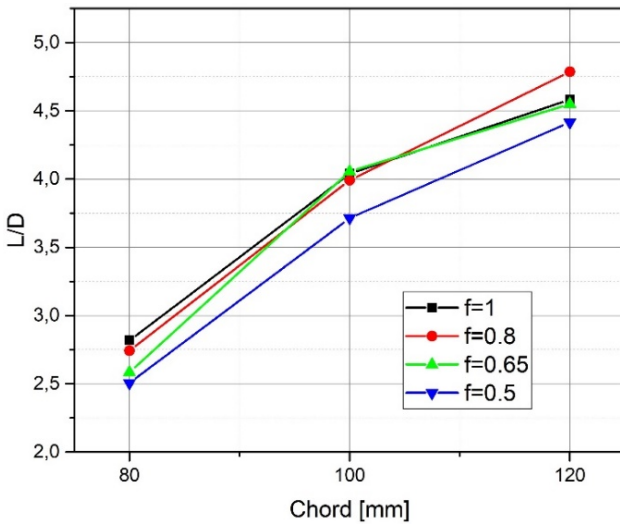


Fig. 21. Effect of f factor on the L/D ratio of the wing

D. Two Sided Tapering

Front and back tapering, or the triangular form, was simulated based on $\beta = -\lambda$, with a tapering factor f of 0.5, 0.65, 0.8, and 1, which is basically the triangular form. The wings in these simulations also have the same area, with $\alpha = 6.5^\circ$. Drag force was shown to decrease with increase of f , the lowest drag force being for the rectangular form, where $f = 1$. Lift force, however, increased with increased f . The highest lift force was generated from the wing with $f = 0.5$. The geometry with the highest L/D was at $f = 0.8$ as shown in Fig. 22.

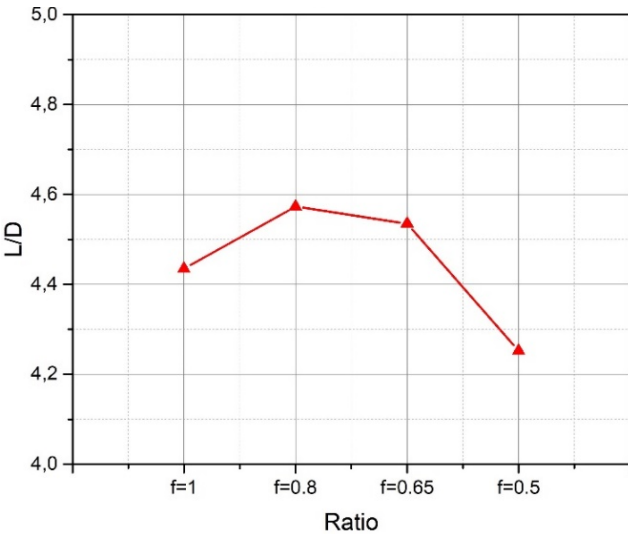


Fig. 22. Two sided tapering effect on the L/D ratio of the wing.

E. Effect of Induced drag

The effect of induced drag was visible at the tip of the wing, a small portion of the fluid moving from the high-pressure side to the lower-pressure side. The effect shown in Fig. 23 results in a loss in pressure difference across the cross-section of the wing, and so a decrease in lift force. This indicates the necessity of adding winglets, which was recommended by [5].

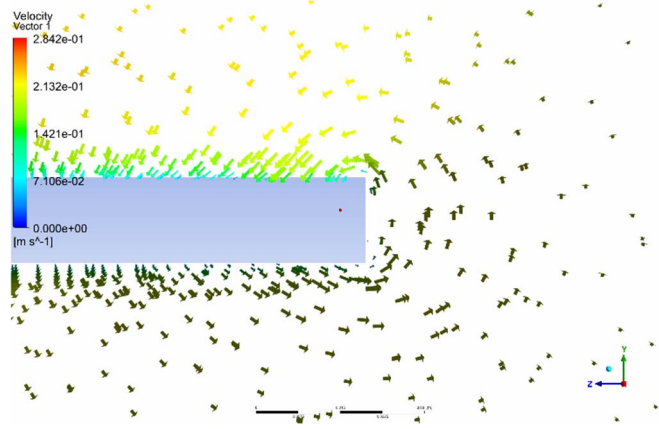


Fig. 23. Effect of induced drag at the tip of the wing

F. Comparison of results

Extra simulations were performed to optimize the shape of the wing and choose the geometry which gives the best hydrodynamic parameters. Some geometries were combined, such as the best cases of sweeping ($\lambda = 15$) and front tapering ($f = 0.65$). Some simulations were repeated but in different areas, to ensure the same area for all geometries. Fig. 24 and 25 show C_D , C_L , and L/D for different geometries. The lowest drag was generated by using the swept wing. The highest lift, and highest lift to drag ratio was generated by the front tapered wing.

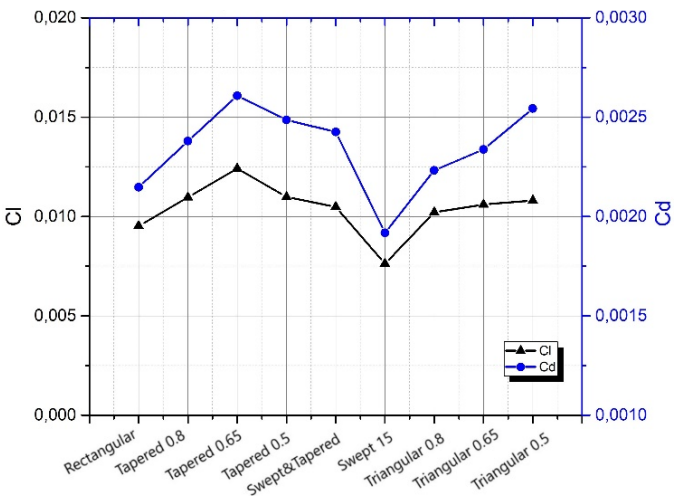


Fig. 24. C_d and C_l of the different shapes simulated

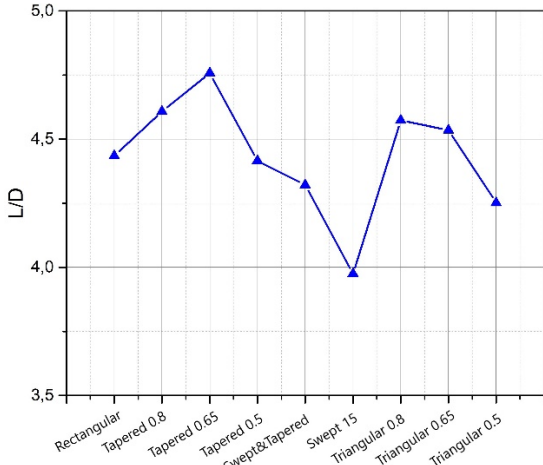


Fig. 25. L/D ratio of different shapes simulated

IV. CONCLUSION

This study was carried out to find the best geometry for the wings of a micro underwater glider for “OASYS” project. The best geometry was found by determining the best NACA cross-section for the wing, the best angle of attack, and the best geometry. The NACA-0016 was selected from five symmetrical cross-sections due to its high lift to drag ratio, and its high stall angle.

The best angle of attack for the selected cross-section was found to be 6.5° . There are two options for achieving this angle during glider flight. The first is movable wings, controlled by the control system of the glider based on feedback from the Inertial Measurement Unit (IMU). The second is to design the rolling movement control mechanism so that it can roll the glider 180° whenever the state of buoyancy is changed. The second solution is more convenient as it does not require any extra mechanisms, motors, or shaft sealings.

The best geometry optimized by two-dimensional and three-dimensional analysis was found to be a tapered geometry with a tapering factor of 0.65. The lift to drag ratio for this was found to be 4.757 .

The simulations clearly showed the effect of induced drag. Induced drag reduced the performance of the wings, by reducing the lift force generated by them. This further emphasizes the importance of adding winglets to the tips of wings.

ACKNOWLEDGMENT

“OASYS” research project is funded by the Research Council of Norway (RCN), the German Federal Ministry of Economic Affairs and Energy (BMWi) and the European Commission under the framework of the ERA-NET Cofund MarTERA.

REFERENCES

- [1] Hobson, Brett W., et al. "Tethys-class long range AUVs-extending the endurance of propeller-driven cruising AUVs from days to weeks." *2012 IEEE/OES autonomous underwater vehicles (AUV)*. IEEE, 2012.
- [2] Sarraf, Christophe, et al. "Thickness effect of NACA foils on hydrodynamic global parameters, boundary layer states and stall establishment." *Journal of Fluids and Structures* 26.4 (2010): 559-578.
- [3] Nordin, Khairul Hanif, Mark Ovinis, and Muhammad Yasar Javaid. "Study on the Effect of Wing Geometry on Underwater Glider Hydrodynamics [J]." *ARPN Journal of Engineering and Applied Sciences* 12.10 (2017): 3101-3104.
- [4] Liu, Fang, et al. "Hydrodynamic performance analysis and experiments of a hybrid underwater glider with different layout of wings." *Oceans 2014-Taipei*. IEEE, 2014.
- [5] Lyu, Da, et al. "Winglet effect on hydrodynamic performance and trajectory of a blended-wing-body underwater glider." *Ocean Engineering* 188 (2019): 106303.
- [6] Claustre, Hervé, and Laurent Begury. "SeaExplorer glider breaks two world records." *Sea Technol* 55.2014 (2014): 19-21.
- [7] Barker, William P. *An Analysis of Undersea Glider Architectures and an Assessment of Undersea Glider Integration into Undersea Applications*. NAVAL POSTGRADUATE SCHOOL MONTEREY CA DEPT OF SYSTEMS ENGINEERING, 2012.
- [8] Dhanak, Manhar R., and Nikolaos I. Xiros, eds. *Springer handbook of ocean engineering*. Springer, 2016.
- [9] Davis, Russ E., Charles C. Eriksen, and Clayton P. Jones. "Autonomous buoyancy-driven underwater gliders." *The technology and applications of autonomous underwater vehicles* (2002): 37-58.
- [10] Airfoil online tool: <http://www.airfoiltools.com/>
- [11] Yunus, A. Cengel. *Fluid Mechanics: Fundamentals And Applications (SI Units)*. Tata McGraw Hill Education Private Limited, 2010.
- [12] Morgado, J., et al. "XFOIL vs CFD performance predictions for high lift low Reynolds number airfoils." *Aerospace Science and Technology* 52 (2016): 207-214.
- [13] Drela, Mark. "XFOIL: An analysis and design system for low Reynolds number airfoils." *Low Reynolds number aerodynamics*. Springer, Berlin, Heidelberg, 1989. 1-12.